

LoCuSS: Exploring the selection of faint blue background galaxies for cluster weak-lensing

Felicia Ziparo^{1*}, Graham P. Smith¹, Nobuhiro Okabe^{2,3}, Chris P. Haines⁴,
Maria J. Pereira⁵, Eiichi Egami⁵

¹ *School of Physics and Astronomy, University of Birmingham, Edgbaston, Birmingham B15 2TT, England*

² *Department of Physical Science, Hiroshima University, 1-3-1 Kagamiyama, Higashi-Hiroshima, Hiroshima 739-8526, Japan*

³ *Kavli Institute for the Physics and Mathematics of the Universe (WPI), Todai Institutes for Advanced Study, University of Tokyo, 5-1-5 Kashiwa*

⁴ *Departamento de Astronomía, Universidad de Chile, Casilla 36-D, Correo Central, Santiago, Chile*

⁵ *Steward Observatory, University of Arizona, 933 North Cherry Avenue, Tucson, AZ 85721, USA*

Accepted... Received... ; in original form...

ABSTRACT

Cosmological constraints from galaxy clusters rely on accurate measurements of the mass and internal structure of clusters. An important source of systematic uncertainty in cluster mass and structure measurements is the secure selection of background galaxies that are gravitationally lensed by clusters. This issue has been shown to be particularly severe for faint blue galaxies. We therefore explore the selection of faint blue background galaxies, by reference to photometric redshift catalogs derived from the COSMOS survey and our own observations of massive galaxy clusters at $z \sim 0.2$. We show that methods relying on photometric redshifts of galaxies in/behind clusters based on observations through five filters, and on deep 30-band COSMOS photometric redshifts are both inadequate to identify safely faint blue background galaxies. This is due to the small number of filters used by the former, and absence of massive galaxy clusters at redshifts of interest in the latter. We therefore develop a pragmatic method to combine both sets of photometric redshifts to select a population of blue galaxies based purely on photometric analysis. This sample yields stacked weak-lensing results consistent with our previously published results based on red galaxies. We also show that the stacked clustercentric number density profile of these faint blue galaxies is consistent with expectations from consideration of the lens magnification signal of the clusters. Indeed, the observed number density of blue background galaxies changes by $\sim 10 - 30$ per cent across the radial range over which other surveys assume it to be flat.

Key words: galaxy: clusters: general – galaxies:general – galaxies:photometry – galaxies:statistics – gravitational lensing:weak

1 INTRODUCTION

Weak gravitational lensing is a direct probe of the projected total mass distribution in galaxy clusters, and is therefore a promising technique for measuring the massive end of the halo mass function (Hoekstra et al. 2013). Such measurements play an important role in a broad range of cosmological studies (Allen et al. 2011), which in turn drives an increasing focus on systematic biases in galaxy cluster mass measurements (e.g. Okabe et al. 2013; Applegate et al. 2014; Hoekstra et al. 2015; Okabe & Smith 2015). Whilst

lensing benefits from the advantage of not requiring assumptions about the nature and physical state of the matter within clusters, there are three principal sources of systematic error: those relating to data reduction and faint galaxy shape measurement, those relating to selection of background galaxies and characterising their redshift distribution, and those relating to the modelling of the shear profile and measuring the underlying halo mass.

Accurate galaxy shape measurements and modelling of cluster mass distributions have both benefited recently from simulations. Building on the initiative taken by the Shear TEsting Programme (STEP Heymans et al. 2006; Massey et al. 2007), faint galaxy shapes can be measured for cluster weak-lensing to an accuracy of $\lesssim 10\%$. Indeed

* E-mail: fziparo@star.sr.bham.ac.uk

some of the more accurate methods are able to achieve few per cent systematics for galaxies as faint as $i \simeq 25$, and also extend the parameter space explored by STEP to include that which is relevant to clusters, i.e. reduced shear of $g \simeq 0.2 - 0.3$ (e.g. Okabe et al. 2013). On the mass modelling side, studies based on cosmological numerical simulations have shown that the ensemble mass calibration of galaxy cluster samples can be recovered to sub-5% accuracy, paying careful attention to modelling details including the range of cluster centric radii over which models are fitted (Bahé et al. 2012; Becker & Kravtsov 2011).

Accurate selection of background galaxies is arguably trickier than the other two sources of systematic error due to the requirement to estimate a robust redshift for a very large number of galaxies many of which are fainter than the limit of the deepest spectroscopic redshift surveys, i.e. $\sim 23 - 26$ th magnitude. Early studies selected faint galaxies in a single photometric band, arguing that faint cluster galaxies are a sub-dominant population (e.g. Kneib et al. 2003; Smith et al. 2005). More recently, colour-magnitude diagrams have been used to exclude galaxies that lie on or close to the ridge line of cluster galaxies – the so-called red sequence (e.g. Okabe et al. 2010; Hoekstra et al. 2012; Applegate et al. 2014), and colour-colour plots have also been used to separate cluster and background galaxy populations (e.g. Limousin et al. 2007; Medezinski et al. 2010; Umetsu et al. 2010; High et al. 2012; Israel et al. 2012). Taking a step further, some authors have attempted to use photometric redshifts of faint galaxies, based on upto 5 photometric bands, e.g. *ugriz* or *BVRiz*, to select background galaxies (e.g. Limousin et al. 2007; Gavazzi et al. 2009; Gruen et al. 2014; Applegate et al. 2014; Covone et al. 2014; McCleary, dell’Antonio & Huwe 2015; Melchior et al. 2015). Given the uncertainties on redshift estimates based on photometry and the faintness of the galaxies in question, none of these methods delivers catalogues of faint galaxies that are free from contamination from foreground and cluster galaxies. Moreover, it is challenging to estimate accurately the contamination level inherent in any given method.

Contamination is generally dominated by faint cluster members, with a cluster centric radial number density profile that is expected to rise towards the cluster centre. A number density profile of background galaxies that is a declining function of cluster centric radius is therefore interpreted as a signature of contamination. Kneib et al. (2003) were the first, to our knowledge, to invoke the assumption that the intrinsic (i.e. uncontaminated) number density profile of background galaxies is flat, and to apply a statistical correction to the measured shear profile to correct for the effects of contamination. This approach has returned to vogue recently (Applegate et al. 2014; Hoekstra et al. 2012, 2015). If the assumption of a flat number density profile of background galaxies is valid for an individual cluster (or an ensemble of clusters when modeling all clusters simultaneously), and if the lens magnification has a negligible effect on the number density of background galaxies, then in principle it should be possible to correct statistically for contamination in this way.

Another approach is to devise colour selection criteria based on photometric redshift catalogues of deep and/or wide blank field surveys. For example early studies used the

Hubble Deep Field observations for this purpose; latterly it is more common to use one of the Cosmological Evolution Survey (COSMOS, e.g. Capak et al. 2007; Ilbert et al. 2006) or CFHT-LS (Hildebrandt et al. 2012) photometric redshift catalogues. The main disadvantage of this approach is that, even if the reference catalogue of redshifts is perfectly accurate, these fields deliberately avoid lines of sight through massive galaxy clusters. Therefore any attempt to estimate the contamination fraction using these catalogues is at best indicative due to the absence, by design, of the troublesome contaminating galaxies at the relevant cluster redshifts. Nevertheless, these methods have been important to improve the accuracy of background galaxy selection.

It is also possible to exploit the lensing signal itself to characterise contamination. These methods rest on the fact that to first order the shapes of contaminating galaxies are uncorrelated with the cluster shear signal and therefore simply reduce the measured signal. Specifically, the reduced tangential shear measured in a given radial bin centred on a cluster is the error weighted sum of reduced tangential shear of each galaxy divided by the sum of the weights. Contaminating galaxies therefore contribute no signal to the numerator and increase the denominator through the weight that is assigned to them. Typically the weight function reflects the measurement uncertainty on the galaxy shape, and not the probability that the galaxy is indeed behind the cluster. The maximal lensing signal is therefore measured from the least contaminated sample of galaxies. Medezinski et al. (2007) therefore introduced the idea of measuring the shear signal of a cluster as a function of colour cut used to define the background galaxy sample, aiming to identify a colour cut beyond which the shear signal saturates. Okabe et al. (2010) applied these methods to 30 galaxy clusters, selecting galaxies redder and bluer than the cluster sequence, for use as background galaxies. Subsequently Okabe et al. (2013) combined this approach with an analytic model of the contamination fraction to achieve 1 per cent contamination in samples of galaxies redder than the cluster red sequence by a colour offset of $\Delta(V-i) \geq 0.475$. Whilst this approach delivered very pure background galaxy samples, it yielded just 5 background galaxies per square arcminute per cluster, i.e. insufficient to measure the mass of individual clusters in their sample. Okabe et al. also found that their techniques produced ambiguous results for blue galaxies, largely because the relationship between colour and redshift is more complicated for blue galaxies than for red galaxies. In a companion to this article, Okabe & Smith (2015) extend Okabe et al.’s red galaxy selection methods to incorporate a colour-cut that depends on clustercentric radius, and thus achieve a number density of 13 galaxies per square arcminute per cluster, again with just 1 per cent contamination.

In this article we investigate several of the issues highlighted above in the context of the Local Cluster Substructure Survey (LoCuSS¹). Our main objective is to explore the selection of blue background galaxies in the $(V-i)/i$ colour-magnitude plane. As outlined above, it is now clear that methods that rely on “saturation” of the shear signal are unreliable for blue galaxies that are selected in this plane. We have therefore obtained *BVRiz*-band data for

¹ <http://www.sr.bham.ac.uk/locuss>

a sub-sample of clusters to study the relationship between photometric redshift, $(V - i)$ colour, and apparent i -band magnitude. The main outcome for our own programme is therefore to assess the reliability of blue galaxy selection. We judge our results based on the target to control systematic biases in LoCuSS weak-lensing mass measurements at the sub-4 per cent level, as set out in Okabe & Smith (2015). We therefore ask the specific question: can we control the contamination of blue background galaxy catalogues at this level? Our approach is based on careful testing of the accuracy of photometric redshifts, and detailed investigation of the limitations of photometric redshifts based on just five photometric bands and/or on blank field observations. This article therefore has broad and significant relevance for the community, in addition to helping us to achieve the goals of LoCuSS.

In §2 we describe the data and the clusters we use for this analysis; in §3 we present the photometric redshift calculation that we then use to define our background galaxy selection method in §4. We discuss our results and conclusions in §5. Throughout our analysis we adopt the following cosmological parameters: $H_0 = 70 \text{ km s}^{-1} \text{ Mpc}^{-1}$, $\Omega_\Lambda = 0.7$, $\Omega_M = 0.3$. All magnitudes are in the AB system.

2 DATA

We use a sample of 50 clusters from the Local Cluster Substructure Survey (LoCuSS), for which sensitive high angular resolution imaging data are available from Suprime-Cam (Miyazaki et al. 2002) on the Subaru 8.2-m telescope²³. The clusters comprise the so-called ‘‘High- L_X ’’ sample and satisfy the following selection from the *ROSAT* All Sky Survey catalogues (Ebeling et al. 1998, 2000; Böhringer et al. 2004) $0.15 \leq z \leq 0.30$, $n_H \leq 7 \times 10^{-20} \text{ cm}^{-2}$, $-25^\circ \leq \delta \leq +65^\circ$, $L_{X[0.1-2.4 \text{ keV}]} / E(z) \geq 4.1 \times 10^{44} \text{ erg s}^{-1}$, where $E(z) = (\Omega_M (1+z)^3 + \Omega_\Lambda)^{0.5}$. This is the same sample as discussed by Okabe et al. (2013), Martino et al. (2014), and Okabe & Smith (2015).

Full details of the Subaru observations, data reduction, photometric calibration, and faint galaxy shape measurements are given by Okabe et al. (2013) and Okabe & Smith (2015). In summary, forty seven clusters were observed through the V - and i' -band filters, and the remaining three through the V/I_C , g/i' , and B/i' -band filters. Our results are insensitive to whether we include or exclude these three clusters. Hereafter we refer to the redder filter as i -band and the bluer filter as V -band. The i -band data were obtained in excellent conditions, with $\text{FWHM}_{\text{median}} = 0.7''$, and typically reach a 5σ point source sensitivity of $i_{\text{AB}} = 26$.

We have also observed three of the fifty clusters through B , R , and z -band filters to allow us to measure photometric redshifts of faint galaxies for this study. These clusters are ABELL0068, ABELL0383 and ABELL0611; they lie at

redshifts $z = 0.251$, $z = 0.188$ and $z = 0.288$, respectively. We have also observed these three clusters with Hectospec (Fabricant et al. 2005) mounted on the Multiple Mirror Telescope (MMT) at Mount Hopkins, Arizona, as part of the Arizona Cluster Redshift Survey (ACReS; Pereira et al., in preparation; see also Haines et al. 2013). ABELL0383 is also covered by the redshift survey of Geller et al. (2014). We assemble a total of 2390 secure spectroscopic redshifts of which 796 are confirmed cluster members. We use these redshifts to train our photometric redshift measurements in §3.2.

3 ANALYSIS

3.1 Photometry

We use the V/i -band photometric catalogues for all 50 clusters from Okabe et al. (2013) and described in detail by Okabe & Smith (2015). Matched BRz -band catalogues are constructed following the same procedures. We adopt the SExtractor (Bertin & Arnouts 1996) parameter `MAG_AUTO` as the total magnitude of each object in the i -band, and measure aperture magnitudes in all bands within apertures matched to $1.5\times$ the worst seeing ($\sim 0.85''$) of the available filters for each cluster, after smoothing each frame to the worst seeing. This approach is well matched to the photometric analysis of COSMOS observations (Ilbert et al. 2006).

We check the reliability of the photometric calibration in two ways. First, we select unsaturated stars with $i > 20$ and `CLASS_STAR` ≥ 0.99 , and compare their colours with those derived from template spectra from Pickles (1998), white dwarves and other stellar types. The observed and synthetic colours match very well and imply residual uncertainties on the photometric calibration at the sub-10 per cent level – i.e. consistent with the calibration analysis of Okabe & Smith (2015). Second, we perform a more quantitative test, using *Le PHARE* (PHotometric Analysis for Redshift Estimations; Arnouts et al. 2001; Ilbert et al. 2006) in ‘‘training mode’’. For objects of known redshift *Le PHARE* recursively computes the systematic offsets for the photometric zero-points (see Ilbert et al. 2006). The resulting shifts are of the order of a few per cent.

3.2 Photometric redshifts

We compute photometric redshifts for all sources detected at $i \leq 26$ in the Suprime-Cam observations of ABELL0068, ABELL0383 and ABELL0611, using ten Spectral Energy Distribution (SED) templates based on multi-wavelength observations of Virgo cluster (Boselli, Gavazzi & Sanvito 2003) and twelve starburst galaxy templates used by COSMOS (Ilbert et al. 2009), and generated with Bruzual & Charlot (2003) stellar population synthesis models. The Virgo templates best represent cluster galaxies at $z \simeq 0.2$ (Ziparo et al. 2012); the COSMOS templates span the range of spectral properties expected of higher redshift galaxies. Dust extinction is applied to all templates bluer than an Sa spectral type using the modified Calzetti et al. (2000) attenuation law with $0 \leq E(B - V) \leq 0.5$ and with a step of $\Delta E(B - V) = 0.1$.

² Based in part on observations obtained at the Subaru Observatory under the Time Exchange program operated between the Gemini Observatory and the Subaru Observatory.

³ Based in part on data collected at Subaru Telescope and obtained from the SMOKA, which is operated by the Astronomy Data Center, National Astronomical Observatory of Japan.

Finally, we add a set of emission lines to the templates following [Ilbert et al. \(2006\)](#).

We test the reliability of the photometric redshifts by comparing them with spectroscopic redshifts from ACREs (§2), defining the catastrophic failure rate, η , following [Ilbert et al.](#), as the fraction of objects for which $|z_{\text{phot}} - z_{\text{spec}}|/(1 + z_{\text{spec}}) > 0.15$. We also compute the accuracy as:

$$\sigma = 1.48 \times \text{median}(|z_{\text{phot}} - z_{\text{spec}}|/(1 + z_{\text{spec}})) \quad (1)$$

following [Ilbert et al. \(2006\)](#). We note [Kelly et al. \(2014\)](#) adopt a different definition of accuracy, preferring to exclude outliers from their calculation. To facilitate comparison with their work, we also compute $\sigma_{\text{Kelly+14}}$, which they define as: the standard deviation of $|z_{\text{phot}} - z_{\text{spec}}|/(1 + z_{\text{spec}})$ after rejecting the outliers with $|z_{\text{phot}} - z_{\text{spec}}|/(1 + z_{\text{spec}}) > 0.1$.

We obtain a photometric redshift accuracy of $\sigma \simeq 0.03 - 0.04$ and a catastrophic failure fraction of $\eta \simeq 0.02 - 0.04$ (left panels in Fig. 1); $\sigma_{\text{Kelly+14}}$ is consistent with σ , for this comparison with spectroscopic redshifts. We also compute $\mu_{\Delta z}$ to test for any systematic over- or under-estimation of redshift, defined thus:

$$\mu_{\Delta z} = \left\langle \frac{z_{\text{phot}} - z_{\text{spec}}}{1 + z_{\text{spec}}} \right\rangle \quad (2)$$

constraining any systematic bias at the $\lesssim 1\%$ level (right panels of Fig. 1). Overall, our tests suggest that for galaxies with sufficiently high S/N, BVRiz photometric redshifts are able to robustly distinguish contaminant cluster galaxies from background ($z > 0.4$) galaxies.

3.3 Photometric redshifts beyond 20th magnitude

The median i-band magnitude of galaxies with ACREs redshift is $i = 19.38$, and 95% of the sources have $i < 20.8$. Therefore, whilst encouraging, the tests described in §3.2 do not examine directly the reliability of galaxies used for weak-lensing mass measurements. We therefore turn to the COSMOS UltraVISTA photometric redshift catalogue ([McCracken et al. 2012](#); [Ilbert et al. 2013](#)) that is limited at $i < 27.5$, and benefits from four deep near-infrared filters Y , J , H and K_S . This filter coverage enables more robust photometric redshifts for galaxies at $z > 1.3$ than earlier versions of the COSMOS catalogue, since the Balmer break is redshifted to the near-infrared for these galaxies. Furthermore, the COSMOS UltraVISTA photometric redshifts are tested against almost 35,000 new spectra with galaxies at $z > 1.5$ (for more details see [Ilbert et al. 2013](#)).

A further advantage of the COSMOS data is that their optical data were obtained with Suprime-Cam at Subaru, allowing a straightforward comparison with our analysis. We therefore use the COSMOS photometry and photometric redshifts (based on 30 photometric bands) to test our method for computing photometric redshifts from BVRiz photometry. We apply the methods described in §3.2 to COSMOS BVRiz photometry and compare the resulting COSMOS 5-band photometric redshifts, z_5 , with COSMOS 30-band photometric redshifts, z_{30} , from [Ilbert et al. \(2013\)](#). Replacing z_{spec} with z_{30} in our definitions of σ , η , and $\mu_{\Delta z}$, we obtain an accuracy, catastrophic failure fraction, and systematic offset of: $\sigma = 0.16$, $\eta = 0.41$, and $\mu_{\Delta z} = -0.07$ respectively (Fig. 2). As expected, BVRiz photometry does not constrain photometric redshifts as well as 30 bands. For

example, the cloud of points at $z_{30} < 1$ and $z_5 > 2.5$ arise from degeneracy between the 4000 Å and Lyman breaks, and similarly at $z_{30} > 1.5$. We note that [Kelly et al. \(2014\)](#) performed a similar test to ours, obtaining $\sigma_{\text{Kelly+14}} = 0.06$ down to $i \simeq 24$. We obtain a similar result – $\sigma_{\text{Kelly+14}} = 0.05$ – if we follow their approach of excluding outliers from the calculation of σ (Fig. 2).

An important caveat on the preceding analysis is that it compares one set of photometric redshifts with another, notwithstanding the fact that the COSMOS filter set is the most complete in the literature at these depths and solid angle. We therefore perform a more refined test of our 5-band photometric redshift methods, taking advantage of the full redshift probability distribution, $P(z)$, from the COSMOS catalogue. [Ilbert et al. \(2006\)](#) noted that the catastrophic failure fraction of galaxies that present a second $P(z)$ peak with a probability greater than 5% is $\eta = 0.44$. This is comparable with our catastrophic failure fraction of $\eta = 0.41$. We therefore select a “pseudo-spectroscopic” sub-sample of COSMOS galaxies that each have a single $P(z)$ peak above a probability of 5%, and obtain $\sigma = 0.04$, $\eta = 0.13$, and $\mu_{\Delta z} = -0.01$ (bottom panels of Fig. 2). This is similar to the comparison with spectroscopic redshifts in §3.2, albeit with a higher catastrophic failure fraction. Note that this restricted sample of galaxies with single peaked $P(z)$ represents just 4% of the total COSMOS sample.

The inability of BVRiz-band photometric redshifts to correctly locate some galaxies at $z \lesssim 0.3$ that was noted above, is seen again in the lower left panel of Fig. 2 – note the galaxies at $z_{30} < 0.3$ and $z_5 > 1$. However the effect is less pronounced than when comparing BVRiz-band photometric redshifts with the full COSMOS sample (upper left panel of Fig. 2), as is reflected in the improved values of σ , η , and $\mu_{\Delta z}$. Indeed, these galaxies are generally blue, with $(V - i) \lesssim 0.5$, and are typical of the galaxies used in many galaxy cluster weak-lensing studies that use colour and/or 5-band photometric redshift selection (e.g. [Okabe et al. 2010](#); [Umetsu et al. 2010](#); [High et al. 2012](#); [Applegate et al. 2014](#); [Hoekstra et al. 2015](#)).

3.4 Summary

We have computed photometric redshifts of galaxies detected within the Suprime-Cam field of view, centred on three massive galaxy clusters at $z \simeq 0.2$. These photometric redshifts are based on deep BVRiz-band observations. We use spectroscopic redshifts from ACREs (§3.2), and photometric redshifts from the COSMOS UltraVISTA catalogue (§3.3) to test the reliability of these 5-band photometric redshifts, obtaining encouraging results. The accuracy is typically $\sigma \simeq 0.04$, the catastrophic failure fraction is $\eta \lesssim 0.1$, and any systematic bias is of the order $\mu_{\Delta z} \simeq 0.01$. Note that our tests using the COSMOS catalogue use a “pseudo-spectroscopic” sub-sample of COSMOS galaxies that have a single peak in their $P(z)$ distribution. Nevertheless, the degeneracy between the spectral shapes of blue galaxies at $z \lesssim 0.3$ and $z \simeq 2 - 3$ is not broken by BVRiz-band photometry, causing concerns regarding contamination of blue background galaxy samples selected based on these bands and photometric redshifts derived from them.

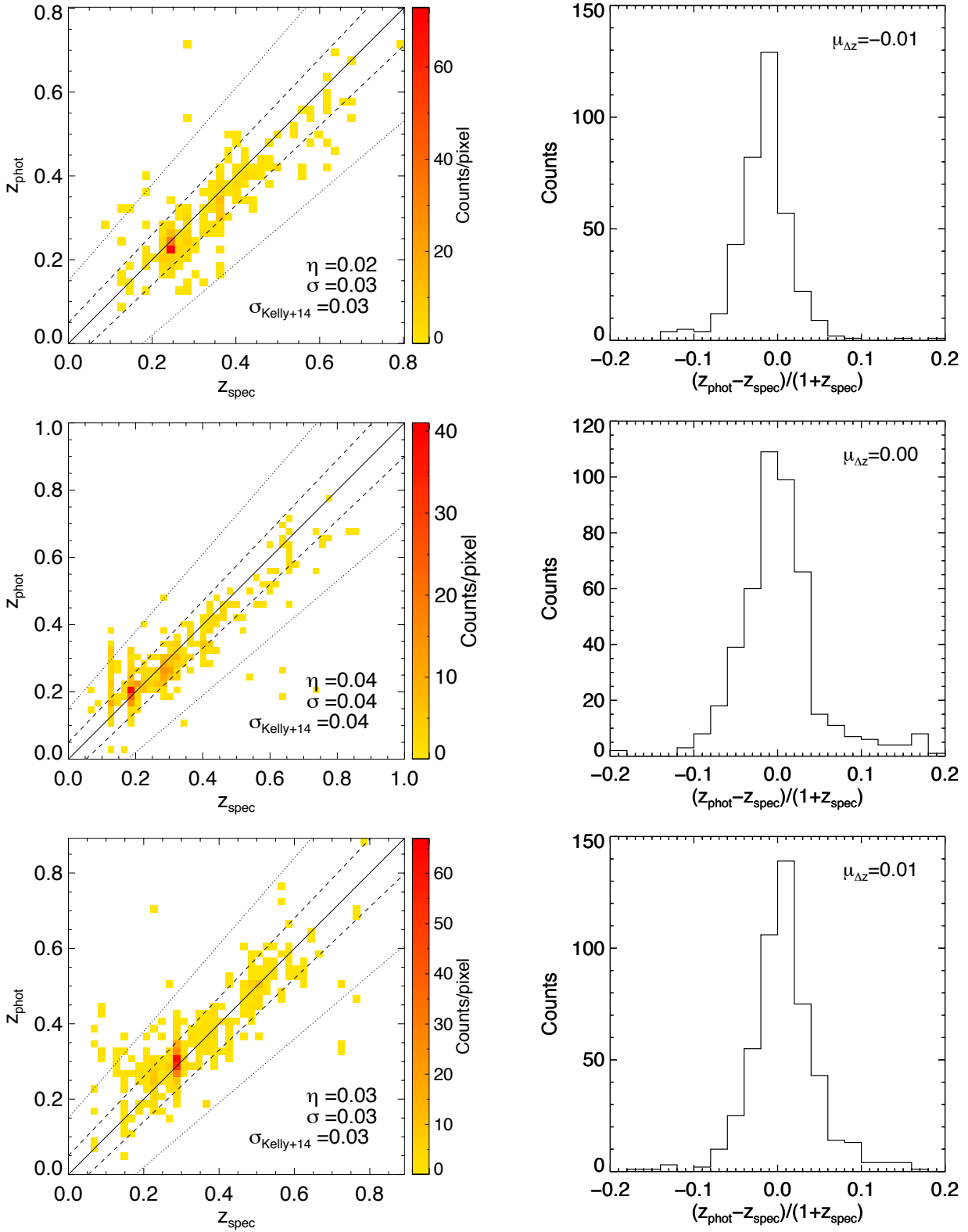


Figure 1. Photometric (z_{phot}) versus spectroscopic redshift (z_{phot} , left panels) and distribution of $(z_{\text{phot}} - z_{\text{spec}})/(1 + z_{\text{spec}})$ (right panels) for ABELL0068, ABELL0383 and ABELL0611 in the top, middle and bottom panels, respectively. The solid lines in the left panels represent $z_{\text{spec}} = z_{\text{phot}}$, while dashed and dotted lines are for $z_{\text{phot}} = z_{\text{spec}} \pm 0.05(1 + z_{\text{spec}})$ and $z_{\text{phot}} = z_{\text{spec}} \pm 0.15(1 + z_{\text{spec}})$, respectively. η is the fraction of catastrophic failures, σ represents the accuracy as computed by Ilbert et al. (2006) and $\sigma_{\text{Kelly+14}}$ is the accuracy as computed by Kelly et al. (2014). The colour bar in the left panels shows the density of points calculated in counts/pixels with red colour highlighting that galaxies are concentrated at the cluster redshift. $\mu_{\Delta z}$ is the mean of the distribution in the right panels.

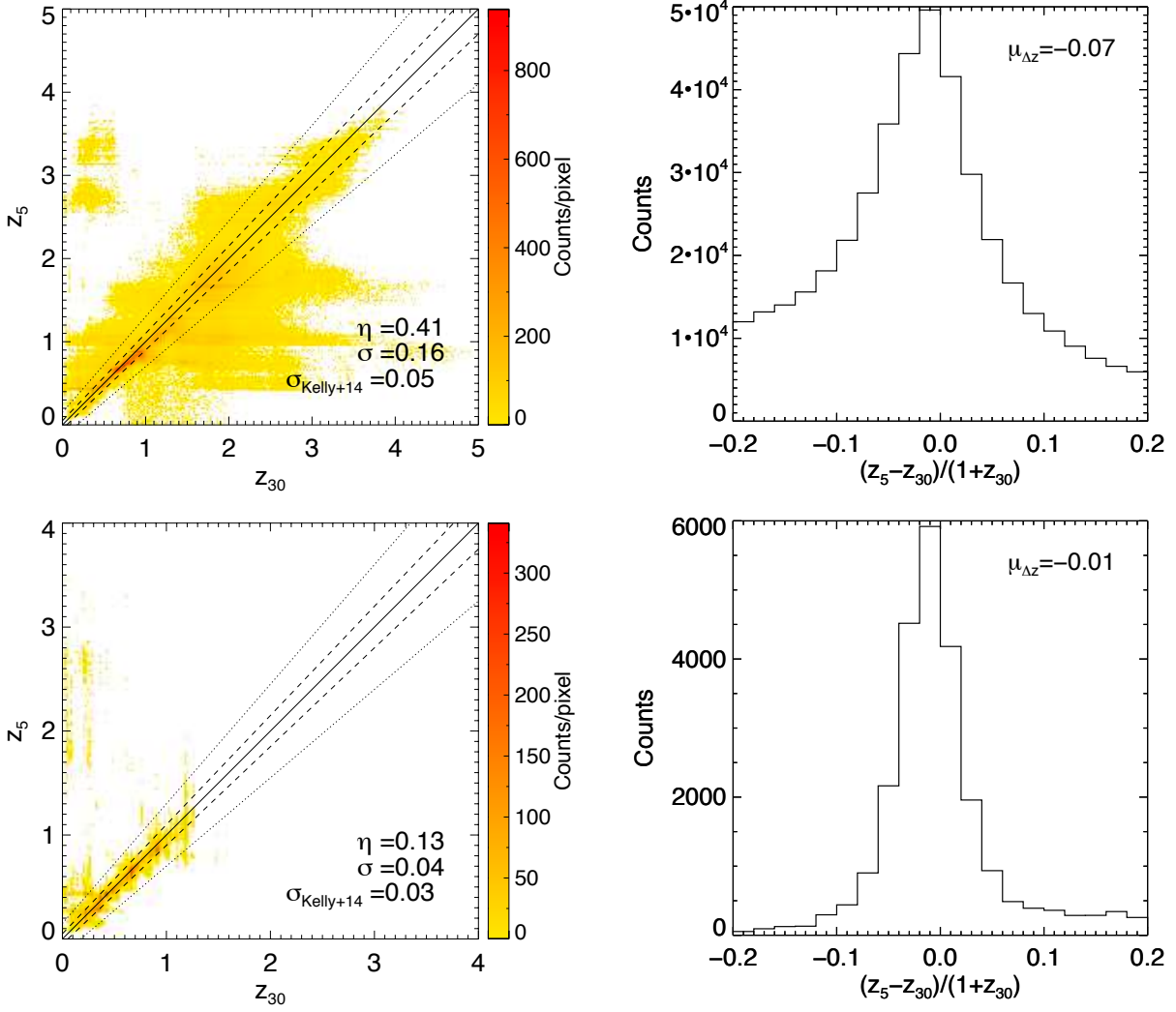


Figure 2. 5-band photometric redshifts z_5 computed in this work versus 30-band photometric redshifts z_{30} from [Ilbert et al. \(2013\)](#) for all galaxies (top left panel) and no more than one peak in the $P(z)$ above a probability of 5% (bottom left panel) in the COSMOS field. The right panels represent the distribution of $(z_5 - z_{30})/(1 + z_{30})$ from the left corresponding panels. All symbols are the same as in Fig. 1.

4 RESULTS

We use the full $P(z)$ distribution of each galaxy in the three photometric redshift catalogues discussed in §3 to investigate the selection of background galaxies for weak-lensing calculations. These catalogues comprise: (1) “LoCuSS” $BVRiz$ -band photometric redshifts of galaxies along the line of sight through ABELL0068, ABELL0383, and ABELL0611 (§3.2); (2) “COSMOS-30” photometric redshifts of galaxies within the 1.5×1.5 degree² footprint of the UltraVISTA observations of the COSMOS field ([Ilbert et al. 2013](#)); (3) “COSMOS-5” $BVRiz$ -band photometric redshifts of galaxies in the same UltraVISTA footprint (§3.3).

We define P_{bkg} as the probability that a galaxy is at a redshift of $z \geq 0.4$, i.e. well beyond the redshift of the clusters considered here, and also beyond the redshift limit of the LoCuSS cluster sample (§2). We compute P_{bkg} for every galaxy in all three catalogues as follows:

$$P_{\text{bkg}} = \frac{\int_{0.4}^{z_{\text{max}}} P(z) dz}{\int_0^{z_{\text{max}}} P(z) dz} \quad (3)$$

where $z_{\text{max}} = 6$ is the maximum redshift considered for the photometric redshift calculations (§§3.2 & 3.3). In the following sections we investigate the utility of different colour and magnitude cuts to define a sample of galaxies that suffers minimal contamination by faint cluster and foreground galaxies. We therefore further define $P_{\text{bkg}}^{\text{bin}}$ as the mean value of P_{bkg} for a given “bin” of $(V-i)/i$ colour-magnitude space: $P_{\text{bkg}}^{\text{bin}} = \langle P_{\text{bkg}} \rangle$. This quantity allows us to link the $P(z)$ information in the three photometric redshift catalogues with the colour-magnitude information that is available for the full LoCuSS sample.

4.1 Redshift as a function of colour and magnitude

We study the photometric redshift distribution of galaxies in the LoCuSS catalogue as a function of $(V-i)$ colour and i -band magnitude. First, we split the colour-magnitude plane up into four regions: red sequence, red, green valley, and faint

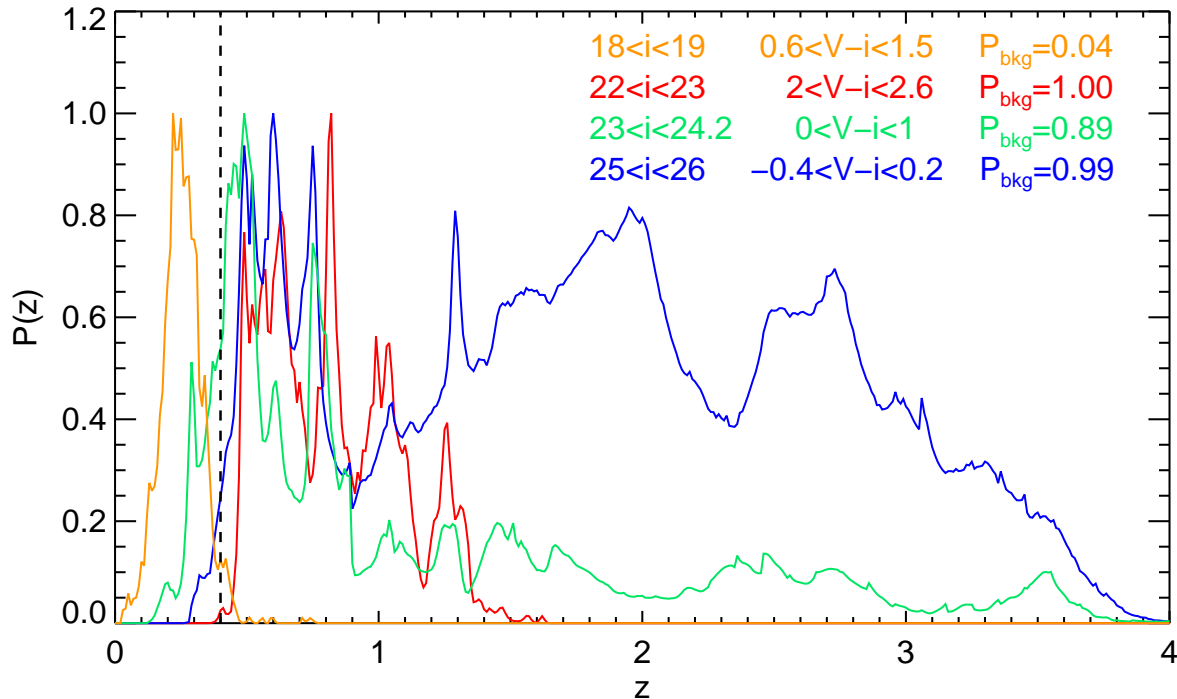


Figure 3. Mean normalised $P(z)$ for different class of galaxies, showing in different colours (see legend) red sequence galaxies, red galaxies (i.e. above the red sequence), green valley galaxies and blue galaxies. The black dashed line, at $z = 0.4$, shows the threshold at which we select background galaxies. N_{gal} indicates the number of galaxies populating each $(V - i)/i$ bin, while P_{bkg} is the integrated probability for those galaxies to be at $z > 0.4$.

blue galaxies. Red sequence galaxies ($0.6 < V - i < 1.5$, $18 < i < 19$) have a well defined $P(z)$ peak at $z \simeq 0.2$ and negligible probability of being background galaxies, $P_{\text{bkg}}^{\text{bin}} = 0.04$ (orange curve in Fig. 3). In contrast, red galaxies ($2.0 < V - i < 2.6$, $22 < i < 23$) suffer negligible contamination by foreground and cluster galaxies, with $P_{\text{bkg}}^{\text{bin}} = 1.00$ (red curve in Fig. 3). This gives independent confirmation of Okabe et al.’s identification of red galaxies in this colour-magnitude plane as a robust low contamination strategy for selecting background galaxies. Note that Okabe et al. (2013) combined the COSMOS photometric redshift catalogue with measurements of the reduced shear as a function of $(V - i)$ colour to define their red colour cut; they did not use the LoCuSS photometric redshift catalogue discussed here.

Moving blueward of the red sequence, we find that the $P(z)$ of green valley galaxies ($0 < V - i < 1$, $23 < i < 24.2$) peaks at $z \simeq 0.5$ and extends down to $z \simeq 0.1$. Indeed, with $P_{\text{bkg}}^{\text{bin}} = 0.89$, green valley galaxies appear to include an appreciable fraction of foreground and cluster galaxies (green curve in Fig. 3). Finally, faint blue galaxies ($-0.4 < V - i < 0.2$, $25 < i < 26$) have a very high probability of being at $z > 0.4$, based on the LoCuSS photometric redshifts, with $P_{\text{bkg}}^{\text{bin}} = 0.99$ (blue curve in Fig. 3). However the tests discussed in §3.3 indicate that this may be an over-estimate.

We also bin the colour-magnitude plane more finely to confirm the stability of these results, finding that the $P(z)$ does not vary strongly between adjacent bins of width several tenths of a magnitude (Fig. A1 and Fig. A2 of Appendix A).

4.2 Integrated $P(z)$ as a function of colour and magnitude

We now investigate $P_{\text{bkg}}^{\text{bin}}$ as a function of colour and magnitude for each of the three photometric redshift catalogues (Fig. 4). We emphasise that the LoCuSS catalogue benefits from the presence of a massive galaxy cluster at $z \simeq 0.2$ in the centre of each of three fields of view (i.e. ABELL0068, ABELL0383, ABELL0611); the COSMOS-30 catalogue lacks massive clusters at $z \simeq 0.2$ and benefits from excellent photometric redshift precision; the COSMOS-5 catalogue enjoys none of the advantages of the other two catalogues, however it aides the interpretation of both of the other two catalogues.

The COSMOS-30 catalogue identifies a broad swathe of colour, $0 \lesssim (V - i) \lesssim 1.5$ as suffering $\gtrsim 5\%$ contamination by galaxies at $z < 0.4$, i.e. $P_{\text{bkg}}^{\text{bin}} \lesssim 0.95$ (bottom panel of Fig. 4). At bluer colours it appears from the COSMOS-30 catalogue that galaxies at $(V - i) \lesssim 0$ and $i > 23$ may suffer contamination at the $\sim 1\%$ level – i.e. competitive with the galaxies at $(V - i) \gtrsim 1.5$ that Okabe et al. (2013) used. Turning to the LoCuSS catalogue, we see that red ($V - i \gtrsim 1.5$) and faint ($i \gtrsim 24.5$) galaxies suffer negligible contamination by galaxies at $z < 0.4$ (top panel of Fig. 4). However it is striking that at $i \gtrsim 24$ the LoCuSS $BVRiz$ -band photometric redshifts are unable to pick out the same population of galaxies at $z < 0.4$ as seen in the COSMOS-30 catalogue. This same feature is also seen in the COSMOS-5 catalogue (top panel of Fig. 4), indicating that it is likely a feature of constraining photometric redshifts with just five

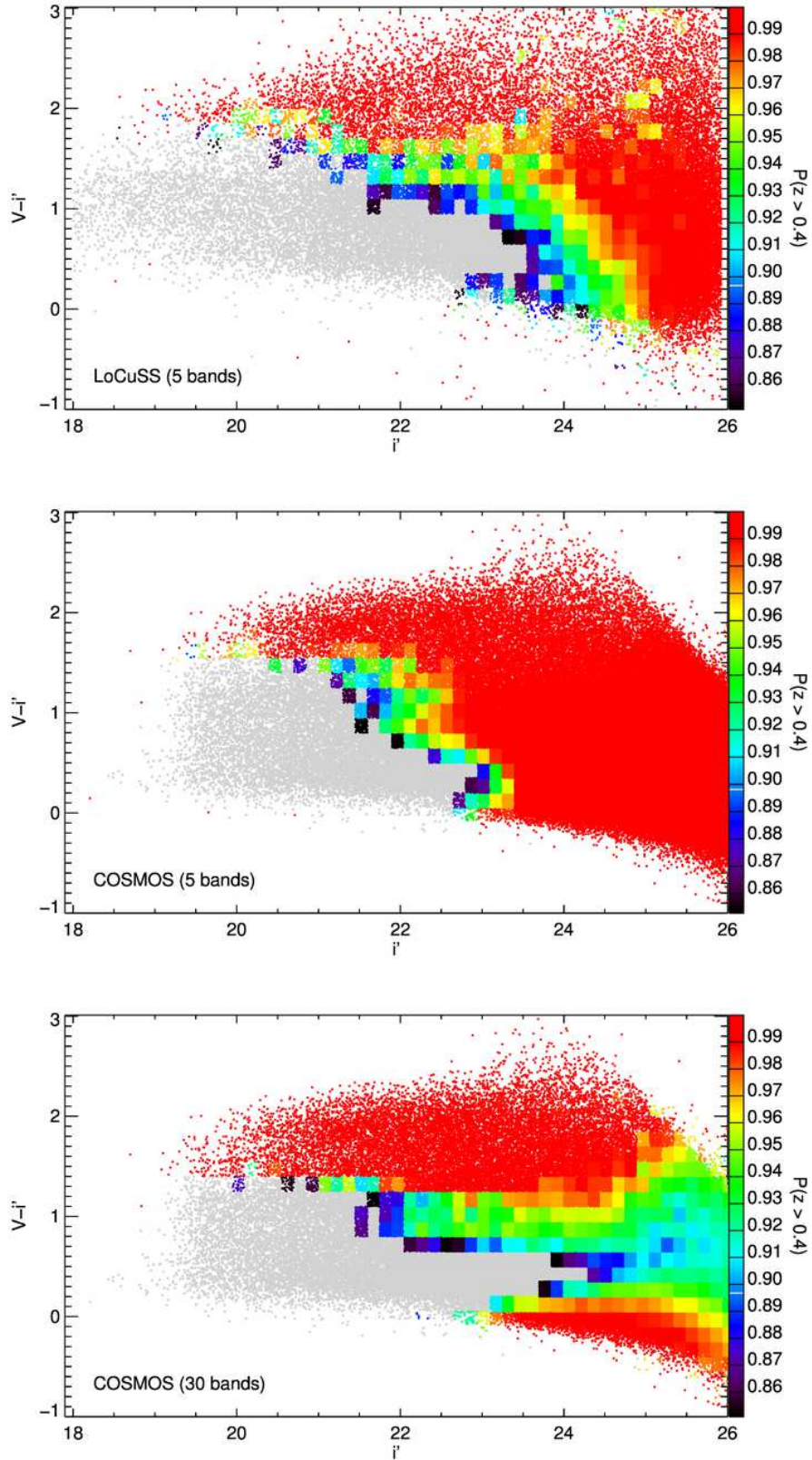


Figure 4. Colour-magnitude diagrams for all sources in the three stacked clusters in LoCuSS (top panel) and for COSMOS (middle and bottom panels). The colour bar represents the probability that a galaxy in a given $(V - i)/i$ bin lies at $z > 0.4$ according to the analysis based on 5 photometric bands (top and middle panels) and 30 bands (bottom panel).

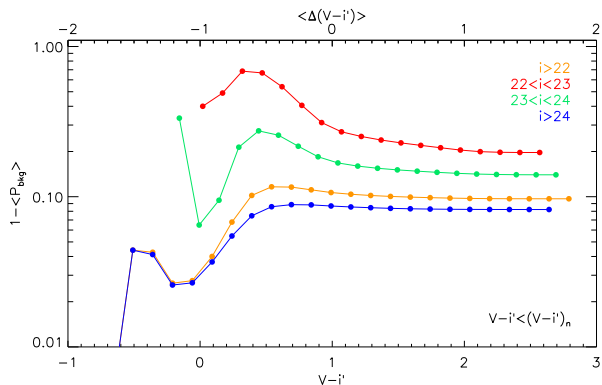


Figure 5. Contamination ($1 - P_{\text{bkg}}$, with P_{bkg} defined in Eq. 3 each galaxy) for all galaxies with $22 < i < 26$ and bluer than a given $(V - i)$ colour, based on the COSMOS-30 catalogue. The top axis of each panel shows the typical $\Delta(V - i)$ from the red sequence of the three clusters in LoCuSS.

photometric bands. Nevertheless, a key difference between the LoCuSS and COSMOS-5 catalogues is that for galaxies bluer than $(V - i) \lesssim 1.5$ – i.e. colours expected to suffer noticeable contamination – the contamination level only falls below $\sim 5\%$ for LoCuSS galaxies at $i \gtrsim 24$, in contrast to the same feature appearing for COSMOS-5 galaxies at $i \gtrsim 23$. We interpret this difference as being caused by the presence of faint cluster and foreground galaxies in the LoCuSS catalogue and absence of the same from the COSMOS catalogues. Combining the strengths of the LoCuSS and COSMOS-30 catalogues therefore suggests that faint blue galaxies satisfying $i \gtrsim 24$ (based on LoCuSS and COSMOS-30) and $(V - i) \lesssim 0.4$ (based on COSMOS-30) should suffer $\lesssim 5\%$ contamination.

4.3 Contamination

We now put the preceding discussion on a firmer quantitative footing and estimate the fraction of faint blue galaxies that are genuine background galaxies. In the absence of a LoCuSS photometric redshift catalogue based on all 30 COSMOS bands, we base our estimates on the COSMOS-30 catalogue because it has the most accurate photometric redshifts, and rely on the LoCuSS catalogue as a sanity check, because it contains clusters at $z \simeq 0.2$. Essentially the LoCuSS photometric redshifts motivate us to consider galaxies fainter than $i = 24$.

Based on the COSMOS-30 catalogues we therefore define contamination as $1 - P_{\text{bkg}}^{\text{bin}} = 1 - \langle P_{\text{bkg}} \rangle$ and investigate how contamination depends on colour and magnitude (Fig. 5). The contamination level for all galaxies at $i > 22$ presents a minimum of $\sim 2 - 3\%$ for the bluest galaxies, i.e. $(V - i) \leq 0$ (orange curve, Fig. 5). However this is dominated by the faintest galaxies, i.e. $i > 24$ (blue curve, Fig. 5), with brighter galaxies suffering contamination upto several tens of per cent (green and red curves, Fig. 5). Our goal of sub-4 per cent systematic biases in LoCuSS weak-lensing mass measurements (Section 1) therefore appears to be achievable with a galaxy selection of $i > 24$ and $(V - i) \lesssim 0$. However this yields < 1 galaxy per square arcminute – i.e. a marginal increase on the number density achieved by Okabe & Smith

(2015). Moreover given the respective limitations of both the COSMOS-30 and LoCuSS photometric redshift catalogues, the measurement of the systematic bias for this blue galaxy selection is less accurate than the measurement of 1 per cent contamination of the red galaxies selected by Okabe & Smith. We therefore conclude that including blue galaxies in the LoCuSS weak-lensing mass measurements of individual clusters is inconsistent with our goal of sub-4 per cent control of systematic biases.

To explore the blue galaxy selection issues further, we adopt an estimated contamination level of 7 per cent as a nominal threshold for selecting blue background galaxies. This is comparable with the level of uncertainty on measurements of systematic biases in other studies in the literature (e.g. Applegate et al. 2014). Whilst this level of contamination exceeds our goals within LoCuSS, it allows us to investigate the radial distribution of the contaminants. Based on the analysis presented in Figure 5, 7 per cent contamination by galaxies at $i > 24$ translates into a colour cut of $V - i < 0.4$, corresponding to a typical difference in colour from the red sequence $\Delta(V - i) = (V - i) - (V - i)_{\text{RS}} < -0.6$. This selection yields a mean number density of 3 galaxies per square arcminute. We use this sample in the following Sections.

4.4 Reduced shear profile and mass modelling

We now probe the mass distribution of the High- L_X sample using the blue background galaxy sample, defined by $i > 24$, $\Delta(V - i) < -0.6$, and using the galaxy shape measurements from Okabe & Smith (2015). These shape measurements are based on methods introduced by (Kaiser, Squires & Broadhurst 1995, the so-called KSB method) using a modified version of the IMCAT package (Okabe et al. 2013; Okabe & Smith 2015). Key features include that we test the reliability of the shape measurement pipeline using simulations that match our observational data and targets. In particular we test our code in the high-shear regime, $g \simeq 0.3$, and simulate data with the same field of view as Suprime-CAM such that we can include sufficient galaxies detected at high signal-to-noise ratio ($\nu > 30$) to test our approach to measuring the isotropic point spread function correction. This is essential to confirm our ability to measure reliable galaxy shapes for galaxies with $i \simeq 25$. Indeed, the multiplicative bias in our shape measurements is just a few per cent and independent of apparent magnitude. Full details are provided in Okabe et al. (2013) and Okabe & Smith (2015); the latter uses a modified version of the former’s shape measurement pipeline. In this article we use the same COSMOS UltraVISTA photometric redshift catalogue as Okabe & Smith, and also use their faint galaxy shape measurements.

We compute the stacked “blue galaxy” reduced shear profile for the full sample of 50 clusters, centred on the respective brightest cluster galaxies (BCGs) following the same approach as Okabe et al. (2013) (Fig. 6). Our blue galaxy shear profile agrees well with Okabe et al.’s red galaxy shear profile at $0.2 - 2h^{-1}$ Mpc, with a slightly lower blue shear signal on smaller scales, and larger signal on larger scales. To quantify the level of agreement, we fit a Navarro, Frenk, & White (1997, NFW) profile to the blue shear profile, obtaining $M_{200} = (7.68_{-0.67}^{+0.71}) \times 10^{14} h^{-1} M_{\odot}$,

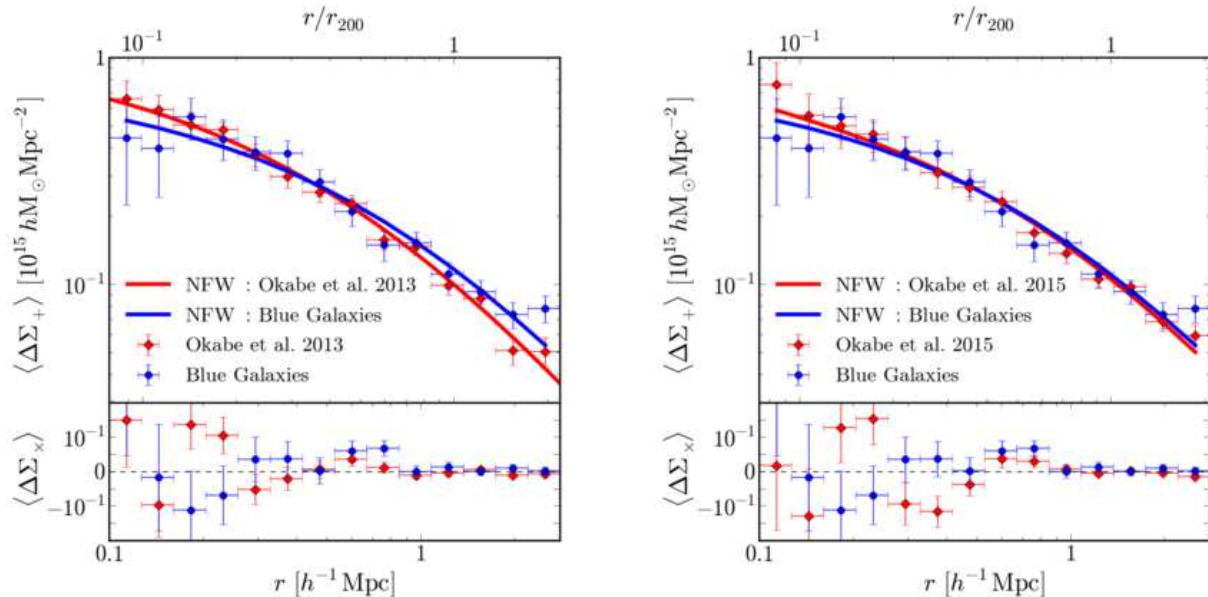


Figure 6. Stacked reduced shear profiles for the full sample of 50 clusters from LoCuSS, using red galaxy selections as in Okabe et al. (2013, left panel) and Okabe & Smith (2015, right panel) and the blue selection as described in this work (both panels). The curves represent the best fit NFW halo to the respective shear profiles, discussed in §4.4.

$c_{200} = 3.06_{-0.28}^{+0.30}$, i.e. higher mass and lower concentration than Okabe et al. (2013) obtained with red galaxies at $\sim 2\sigma$ significance. However a more faithful like-for-like comparison is between our blue galaxy fit and a fit to the new Okabe & Smith (2015) red background galaxy sample, because it is based on the same updated version of the shape measurement pipeline and the same COSMOS UltraVISTA photometric redshift catalogue. Note that our fit to the blue galaxies and the Okabe et al. (2013) fit discussed above both fit a single NFW halo to the data. Okabe & Smith (2015) fit a model comprising an NFW halo, a point mass to represent the brightest cluster galaxy, and a two-halo term to their red galaxy shear profile. Here, to facilitate a direct comparison with Okabe et al. (2013) and our blue galaxy shear profile fit, we fit solely an NFW halo to Okabe & Smith’s red galaxy shear profile. We obtain $M_{200} = (7.14_{-0.42}^{+0.44}) \times 10^{14} h^{-1} M_\odot$, $c_{200} = 3.39_{-0.25}^{+0.26}$, in excellent agreement with our blue galaxy result – the discrepancy is reduced to $\lesssim 1\sigma$. The better agreement in the NFW model fits can be traced to the good agreement of the blue and red shear profiles on scales of a few Mpc (Fig. 6).

4.5 Faint blue galaxy distribution

We further test the reliability of the blue background galaxy catalogue by examining the angular distribution of these galaxies. Ignoring the effects of lensing magnification, the distribution of background galaxies should display no correlation with the location of the foreground galaxy clusters. We find that the observed number density of blue galaxies drops towards the centre of the clusters, and any drop in the number density of red galaxies (defined as in Okabe et al. 2013) is much less pronounced (Fig. 7). A more quantitative view is obtained from the stacked cluster centric num-

ber density profile of the blue and red galaxy samples, revealing that the radial distribution of red galaxies is consistent with being flat and a statistically significant drop is detected in the blue galaxy profile (Fig. 8). To interpret this behaviour robustly requires consideration of the lensing magnification, which acts to boost the sensitivity of the observations through the central cluster regions, at the expense of reducing the intrinsic solid angle that is probed by the data. We compute the run of number density of background galaxies expected from an intrinsically flat distribution of galaxies located behind the clusters, adopting the best-fit NFW profile to the red galaxies as our best estimate of the mean cluster mass distribution. We compute the density (κ) and shear (γ) profiles of this model using the formalism provided by Wright & Brainerd (2000) and from these profiles obtain the magnification profile:

$$\mu(\theta) = \frac{1}{(1 - \kappa(\theta))^2 - \gamma(\theta)^2}. \quad (4)$$

The magnification profile encodes how the presence of the foreground clusters modify both the intrinsic solid angle probed by the observations and the photometric depth of the data. The former is a straightforward factor by which we multiply the solid angle of each radial bin. The latter is taken account of by adjusting the photometric limit down to which we count galaxies as a function of cluster centric radius:

$$i_{\text{limit}}(\theta) = i_0 + 2.5 \log(\mu(\theta)) \quad (5)$$

where i_0 is the unlensed depth of the data, and i_{limit} is the limit after correcting for lensing magnification. To ensure the accuracy of our calculations we implement two additional steps in the selection of background galaxies. Firstly, we select galaxies from those for which Okabe & Smith (2015) have measured a shape, as opposed to the full V/i -band

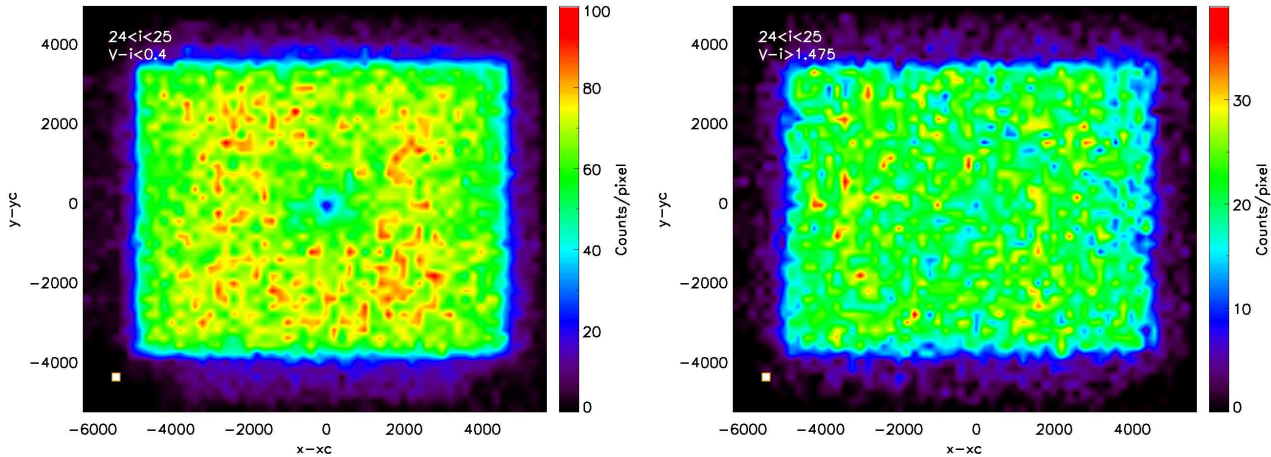


Figure 7. Density map of faint ($24 < i < 25$) blue ($V - i < 0.4$, left panel) and red ($V - i > 1.475$, right panel) galaxies with a shape measurement for 50 clusters. The orange and white square at the bottom left of each panel shows the bin size used to compute the density maps. The colour bar indicates the number of galaxies per pixel in each panel.

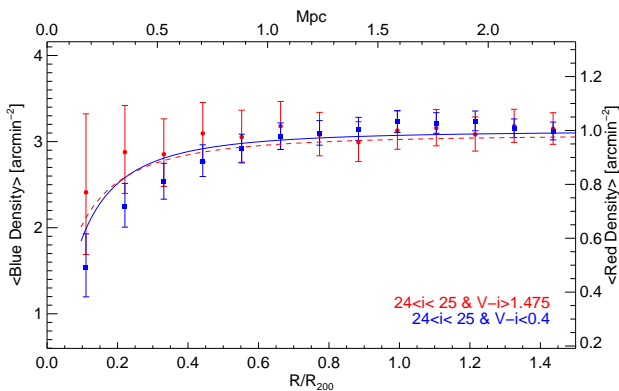


Figure 8. Stacked number density profile of red and blue galaxies behind 50 clusters in the High- L_X cluster sample. Red-dashed line and blue solid line represent the prediction for red and blue galaxies, respectively, based on the magnification modelling described in the text. The two profiles are normalised to the mean density of blue galaxies at $R > R_{200}$.

photometric catalogue. Secondly, we restrict the selection of observed galaxies in the regime of negligible magnification (i.e. $\mu = 1$) to $i_0 = 25$, i.e. a full magnitude brighter than the nominal depth of our data. This is important, to ensure that when we compute the expected number density of galaxies at $\mu > 1$, we do so down to a value of i_{limit} that does not suffer incompleteness. Note that at projected cluster centric radii of $R \gtrsim 150$ kpc we obtain $i_{\text{limit}} - i_0 \lesssim 0.5$ magnitudes.

The magnification bias is expressed in terms of the number density of background galaxies as $n_\mu = n_0 \mu^{2.5s-1}$ where n_0 is the unlensed mean surface number density of background galaxies, μ is the magnification and s is the slope of the number counts of galaxies in the cluster outskirts ($R > R_{200}$). For the faint limit used in this work ($i \sim 25$) we find a slope $s = 0.12$ for red galaxies and $s = 0.22$ for blue galaxies. In both cases, the slopes are less than the lensing invariant slope $s = 0.4$ implying a deficit of background galaxies.

Both red and blue galaxies are consistent with the model prediction within the errors (Fig. 8), albeit with a possible deficit of blue galaxies relative to the model at $R \lesssim 0.5$ Mpc. However the amplitude of this possible deficit is comparable with the fractional decrease in the observed solid angle per bin due to obscuration by bright cluster galaxies (Umetsu et al. 2014), we therefore do not regard this difference as significant. Note that we have not corrected the data points in Fig. 8 for this effect.

The apparently flat profile of red galaxies in Fig. 8 might suggest a tension with the typical use of red galaxies for count-depletion measurements, (e.g. Medezinski et al. 2013; Umetsu et al. 2012). In fact, these authors use a population of faint ($z' \lesssim 25$), $R - z'$ red ($R - z' \sim 1$), but $B - R$ blue ($B - R \lesssim 0.5$) galaxies from deep BRz' imaging (e.g., Medezinski et al. 2013, figure 2, table 3; Umetsu et al. 2012, figure 3, table 3). Although the $N(z)$ of their BRz' red galaxies peaks around $z = 1$ (Umetsu et al. 2010, their figure 7) there might be an overlap with our blue population (see Fig. 3), i.e. the red galaxies selected on $(V - i)/i$ colours are not necessarily the same population of galaxies selected in the BRz' space.

Finally, we note that the magnification model curves for both red and blue galaxies show a gentle dependence on cluster centric radius. Based on our data and sample, we find that the observed number density of galaxies that obey an intrinsically flat radial distribution declines by a factor of 1.29 between 2 Mpc and 0.5 Mpc and a factor of 1.07 between 3 Mpc and 0.75 Mpc – i.e. on the respective scales on which Hoekstra et al. (2012) and Applegate et al. (2014) both assume that the *observed* number density profile of background galaxies is flat.

5 SUMMARY AND DISCUSSION

We have tested the reliability of photometric redshifts as a tool for selecting background galaxies for galaxy cluster weak-lensing mass measurements. Our main motivation is

that contamination of background galaxy samples by faint foreground and cluster galaxies is one of the major sources of systematic uncertainty in this field. In particular, we investigate the robustness of photometric redshifts based on five photometric filters (that is common on the literature) for cluster weak-lensing, the dependence of our results on galaxy colour, and run of background galaxy number density with clustercentric radius. These tests are important for our own programme of weak-lensing mass measurements using V - and i -band data within the Local Cluster Substructure Survey (LoCuSS), and generally applicable to other surveys that select from colour-colour planes, one or more colour-magnitude planes, and/or photometric redshift catalogues based on five photometric bands (e.g. [High et al. 2012](#); [Applegate et al. 2014](#); [Hoekstra et al. 2015](#)). In summary, our main results are as follows:

(i) We use a deep spectroscopic catalogue from ACRoS and the COSMOS catalogue to test our photometric redshifts that are derived from $BVRiz$ -band Subaru observations of three galaxy clusters at $z \simeq 0.2$. Our redshifts are accurate in the mean to $\sigma \simeq 0.04$, suffer negligible bias $|\mu_{\Delta z}| \lesssim 0.01$, and a catastrophic failure rate of $\eta \lesssim 0.1$. This is competitive with other surveys that derive photometric redshifts from similar data for the purpose of selecting background galaxies.

(ii) We confirm that the selection of galaxies redder than the red sequence of cluster members by $\Delta(V - i) \geq 0.475$ suffer sub per cent contamination by faint foreground and cluster galaxies, in particular galaxies at $z_{\text{phot}} < 0.4$. This provides independent support for the red galaxy selection methods developed by [Okabe et al. \(2013\)](#).

(iii) In contrast, faint blue galaxies are difficult to place accurately along the line of sight through clusters due to our inability to break the degeneracy between the spectral shape of blue galaxies at $z \lesssim 0.3$ and at $z \simeq 2 - 3$. This highlights the importance of deep u -band photometry.

(iv) We compare LoCuSS photometric redshifts and COSMOS photometric redshifts and find that neither are adequate on their own to identify a low contamination region of $(V - i)/i$ colour magnitude space for selection of blue background galaxies. The LoCuSS redshifts suffer from limited photometric bands, and whilst the COSMOS redshifts benefit from 30 photometric bands, the COSMOS field does not contain any massive galaxy clusters at $z \simeq 0.2$. This is an important result, because it is common in the literature either to use the COSMOS catalogue to calibrate the reliability and redshift distribution of colour-selected galaxy samples (e.g. [Okabe et al. 2010](#)), or to base the selection of background galaxies purely on photometric redshifts derived from 5 photometric filters (e.g. [Applegate et al. 2014](#)). Similarly, photometric redshift catalogues based on 5 filter observations of blank fields, for example the 5-band COSMOS catalogue that we compute, or the CFHTLenS catalogue used by [High et al. \(2012\)](#) and [Hoekstra et al. \(2012\)](#) suffer from limited photometric coverage and absence of clusters from the photometric redshift catalogue.

(v) We combine the strengths of the LoCuSS and COSMOS photometric redshift catalogues to identify a region of colour-magnitude space at $i > 24$, $(V - i) < 0.4$ (corresponding to 0.6 magnitudes bluer than the typical cluster red sequence at $z \simeq 0.2$) in which data and spectral mod-

els are consistent with contamination of colour-selected blue background galaxy samples being ~ 7 per cent. We apply this blue galaxy selection to measure the stacked reduced shear profile of the full High- L_X LoCuSS cluster sample. The best-fit [Navarro, Frenk, & White \(1997\)](#) density profile has a mass and concentration that is consistent with the red galaxy shear profile-based results of [Okabe et al. \(2013\)](#) within $\sim 2\sigma$ and [Okabe & Smith \(2015\)](#) within $\lesssim 1\sigma$. The comparison between our results and the latter study is more like-for-like than with the former.

(vi) We further explore contamination by examining the radial number density profile of colour-selected blue and red galaxies, obtaining a red galaxy profile that is consistent with being flat across the full range of clustercentric radii probed, and a blue galaxy profile that dips by a factor of ~ 2 towards the central cluster region. Both number density profiles are consistent with that expected from consideration of the lensing magnification of the foreground clusters and the slope of the number counts of faint red and blue galaxies measured securely brighter than our detection limit. Our data are therefore consistent with negligible radial trend in the level of contamination suffered by red and blue galaxy samples.

(vii) Recent studies have corrected the slope of their observed number density profile of background galaxies to be radially flat whilst implicitly assuming that lensing magnification has a negligible affect on the number density profile. Our analysis suggests that this assumption is not valid. Certainly, for our sample and data, we find that the observed number density of galaxies that obey an intrinsically flat radial distribution declines by a factor of 1.29 between 2 Mpc and 0.5 Mpc and a factor of 1.07 between 3 Mpc and 0.75 Mpc – i.e. the radial ranges adopted by [Hoekstra et al. \(2015\)](#) and [Applegate et al. \(2014\)](#) respectively.

In the context of LoCuSS, our specific goal was to investigate the feasibility of including faint blue galaxies in the LoCuSS weak-lensing analysis whilst maintaining the systematic bias from contamination at a level sub-dominant to the statistical uncertainties. With a sample of 50 clusters, and typical weak-lensing mass measurement error of 30 per cent, this equates to aiming to control contamination at the sub-4 per cent level. Given the absence of massive galaxy clusters from the COSMOS-30 photometric redshift catalogue, and the shortcomings of 5-band photometric redshift catalogues of clusters that we (and other surveys) have at our disposal, we concluded that this goal is not achievable. [Okabe & Smith \(2015\)](#) therefore base their weak-lensing mass measurements solely on red galaxies, taking advantage of their new radially-dependent red galaxy selection to achieve 13 galaxies per square arcminute and 1 per cent contamination.

ACKNOWLEDGMENTS

We thank Olivier Ilbert and Peter Capak for making the latest version of the photometric COSMOS catalogue available. We thank Keiichi Umetsu, Sean McGee, Walter del Pozzo and Trevor Sidery for useful discussions, and thank Maggie Lieu and Rossella Martino for assistance. We also acknowledge stimulating and cordial discussions with Douglas Applegate, Anja von der Linden, Adam Mantz, and

Henk Hoekstra. FZ and GPS acknowledge support from the Science and Technology Facilities Council. GPS acknowledges support from the Royal Society. NO (26800097) is supported by a Grant-in-Aid from the Ministry of Education, Culture, Sports, Science, and Technology of Japan, and Core Research for Energetic Universe in Hiroshima University (the MEXT program for promoting the enhancement of research universities, Japan). This work was supported by “World Premier International Research Center Initiative (WPI Initiative)” and the Funds for the Development of Human Resources in Science and Technology under MEXT, Japan. CPH was funded by CONICYT Anillo project ACT-1122.

REFERENCES

- Allen S. W., Evrard A. E., Mantz A. B., 2011, *ARA&A*, 49, 409
 Applegate D. E., et al., 2014, *MNRAS*, 439, 48
 Arnouts S., et al., 2001, *A&A*, 379, 740
 Bahé Y. M., McCarthy I. G., Crain R. A., Theuns T., 2012, *MNRAS*, 424, 1179
 Becker M. R., Kravtsov A. V., 2011, *ApJ*, 740, 25
 Bartelmann M., 2010, *CQGra*, 27, 233001
 Bertin E., Arnouts S., 1996, *A&AS*, 117, 393
 Böhringer H., et al., 2000, *ApJS*, 129, 435
 Böhringer H., et al., 2004, *A&A*, 425, 367
 Boselli A., Gavazzi G., Sanvito G., 2003, *A&A*, 402, 37
 Bruzual G., Charlot S., 2003, *MNRAS*, 344, 1000
 Calzetti D., Armus L., Bohlin R. C., Kinney A. L., Koornneef J., Storchi-Bergmann T., 2000, *ApJ*, 533, 682
 Capak P., et al., 2007, *ApJS*, 172, 99
 Covone G., Sereno M., Kilbinger M., Cardone V. F., 2014, *ApJ*, 784, L25
 Ebeling H., Edge A. C., Böhringer H., Allen S. W., Crawford C. S., Fabian A. C., Voges W., Huchra J. P., 1998, *MNRAS*, 301, 881
 Ebeling H., Edge A. C., Allen S. W., Crawford C. S., Fabian A. C., Huchra J. P., 2000, *MNRAS*, 318, 333
 Fabricant D., et al., 2005, *PASP*, 117, 1411
 Gavazzi R., Adami C., Durret F., Cuillandre J.-C., Ilbert O., Mazure A., Pelló R., Ulmer M. P., 2009, *A&A*, 498, L33
 Geller, M. J., Hwang H. S., Diaferio A., Kurtz M. J., Coe D., Rines, K. J., 2014, *ApJ*, 783, 52
 Gruen D. et al., 2014, *MNRAS*, 442, 1507
 Haines C. P., et al., 2013, *ApJ*, 775, 126
 Heymans C., et al., 2006, *MNRAS*, 368, 1323
 High F. W., et al., 2012, *ApJ*, 758, 68
 Hildebrandt H., et al., 2012, *MNRAS*, 421, 2355
 Hoekstra H., Mahdavi A., Babul A., Bildfell C., 2012, *MNRAS*, 427, 1298
 Hoekstra H., Bartelmann M., Dahle H., Israel H., Limousin M., Meneghetti M., 2013, *SSRv*, 177, 75
 Hoekstra H., Herbonnet R., Muzzin A., Babul A., Mahdavi A., Viola M., Cacciato M., 2015, *MNRAS*, 449, 685
 Ilbert O., et al., 2006, *A&A*, 457, 841
 Ilbert O., et al., 2009, *ApJ*, 690, 1236
 Ilbert O., et al., 2013, *A&A*, 556, A55
 Israel H., Erben T., Reiprich T. H., Vikhlinin A., Sarazin C. L., Schneider P., 2012, *A&A*, 546, AA79
 Kaiser N., Squires G., 1993, *ApJ*, 404, 441
 Kaiser, N., Squires, G., & Broadhurst, T. 1995, *ApJ*, 449, 460
 Kelly P. L., et al., 2014, *MNRAS*, 439, 28
 Kitayama T., Suto Y., 1997, *ApJ*, 490, 557
 Kneib J.-P., et al., 2003, *ApJ*, 598, 804
 Lilly S. J., et al., 2007, *ApJS*, 172, 70
 Lilly S. J., et al., 2009, *ApJS*, 184, 218
 Limousin M., et al., 2007, *ApJ*, 668, 643
 McCleary J., dell’Antonio I., Huwe P., 2015, *ApJ*, 805, 40
 Martino R., Mazzotta P., Bourdin H., Smith G. P., Bartalucci I., Marrone D. P., Finoguenov A., Okabe N., 2014, *MNRAS*, 443, 2342
 Massey R., et al., 2007, *MNRAS*, 376, 13
 Medezinski E., et al., 2007, *ApJ*, 663, 717
 Medezinski E., Broadhurst T., Umetsu K., Oguri M., Rephaeli Y., Benítez N., 2010, *MNRAS*, 405, 257
 Medezinski E., et al., 2013, *ApJ*, 777, 43
 Melchior P. et al., 2015, *MNRAS*, 449, 2219
 McCracken H. J. et al., 2012, *A&A*, 544, 156
 Miyazaki S., et al., 2002, *PASJ*, 54, 833
 Navarro R., Bartelmann M., 1996, *astro*, arXiv:astro-ph/9606001
 Navarro, J. F., Frenk, C. S., & White, S. D. M. 1997, *ApJ*, 490, 493
 Oguri M., Bayliss M. B., Dahle H., Sharon K., Gladders M. D., Natarajan P., Hennawi J. F., Koester B. P., 2012, *MNRAS*, 420, 3213
 Okabe N., Umetsu K., 2008, *PASJ*, 60, 345
 Okabe N., Takada M., Umetsu K., Futamase T., Smith G. P., 2010, *PASJ*, 62, 811
 Okabe N., Bourdin H., Mazzotta P., Maurogordato S., 2011, *ApJ*, 741, 116
 Okabe N., Smith G. P., Umetsu K., Takada M., Futamase T., 2013, *ApJ*, 769, L35
 Okabe N., Smith G. P., 2015, *MNRAS*, submitted
 Pickles A. J., 1998, *PASP*, 110, 863
 Popesso P., Biviano A., Böhringer H., Romaniello M., Voges W., 2005, *A&A*, 433, 431
 Scoville N., et al., 2007, *ApJS*, 172, 1
 Smith G. P., Kneib J.-P., Smail I., Mazzotta P., Ebeling H., Czoske O., 2005, *MNRAS*, 359, 417
 Umetsu K., Medezinski E., Broadhurst T., Zitrin A., Okabe N., Hsieh B.-C., Molnar S. M., 2010, *ApJ*, 714, 1470
 Umetsu K., et al., 2012, *ApJ*, 755, 56
 Umetsu K., et al., 2012, *ApJ*, 755, 56
 Umetsu K., et al., 2014, *ApJ*, 795, 163
 Vikhlinin A., et al., 2009, *ApJ*, 692, 1060
 White S. D. M., Navarro J. F., Evrard A. E., Frenk C. S., 1993, *Natur*, 366, 429
 Wright C. O., Brainerd T. G., 2000, *ApJ*, 534, 34
 Ziparo F., Braglia F. G., Pierini D., Finoguenov A., Böhringer H., Bongiorno A., 2012, *MNRAS*, 420, 2480

APPENDIX A: P(Z) AS A FUNCTION OF COLOUR AND MAGNITUDE

This paper has been typeset from a $\text{\TeX}/\text{\LaTeX}$ file prepared by the author.

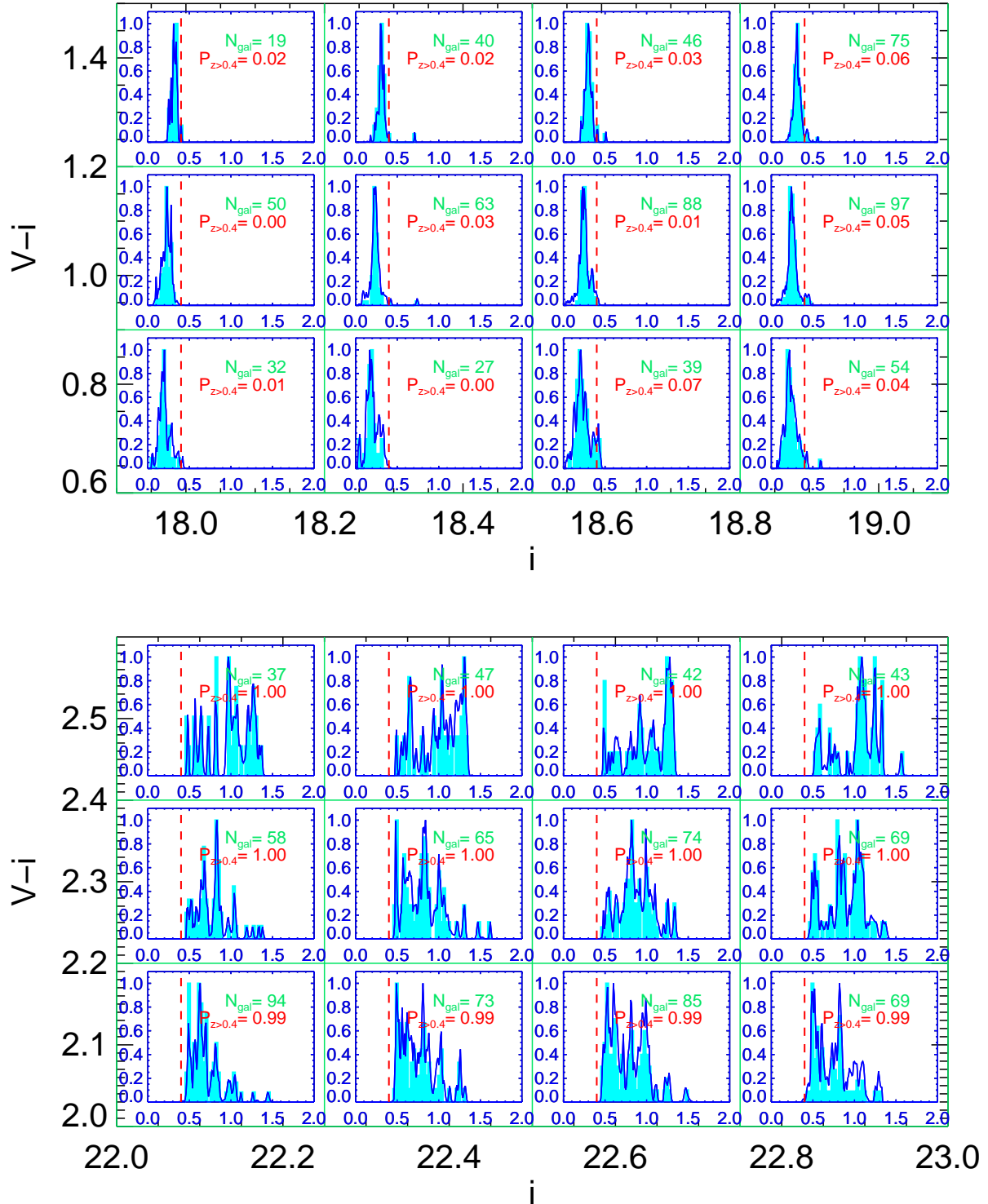


Figure A1. Multi-dimensional analysis in the colour-magnitude space for red sequence (top panel) and red galaxies (i.e. above the red sequence, bottom panel). The blue solid line indicates the average $P(z)$ as a function of redshift in the colour-magnitude cell, while the cyan histogram represents the normalised redshifts distribution of all galaxies in a given cell. The red dashed line, at $z = 0.4$, shows the threshold at which we select background galaxies. N_{gal} indicates the number of galaxies populating each cell, while $P_{z>0.4}$ is the integrated probability for those galaxies to be at $z > 0.4$.

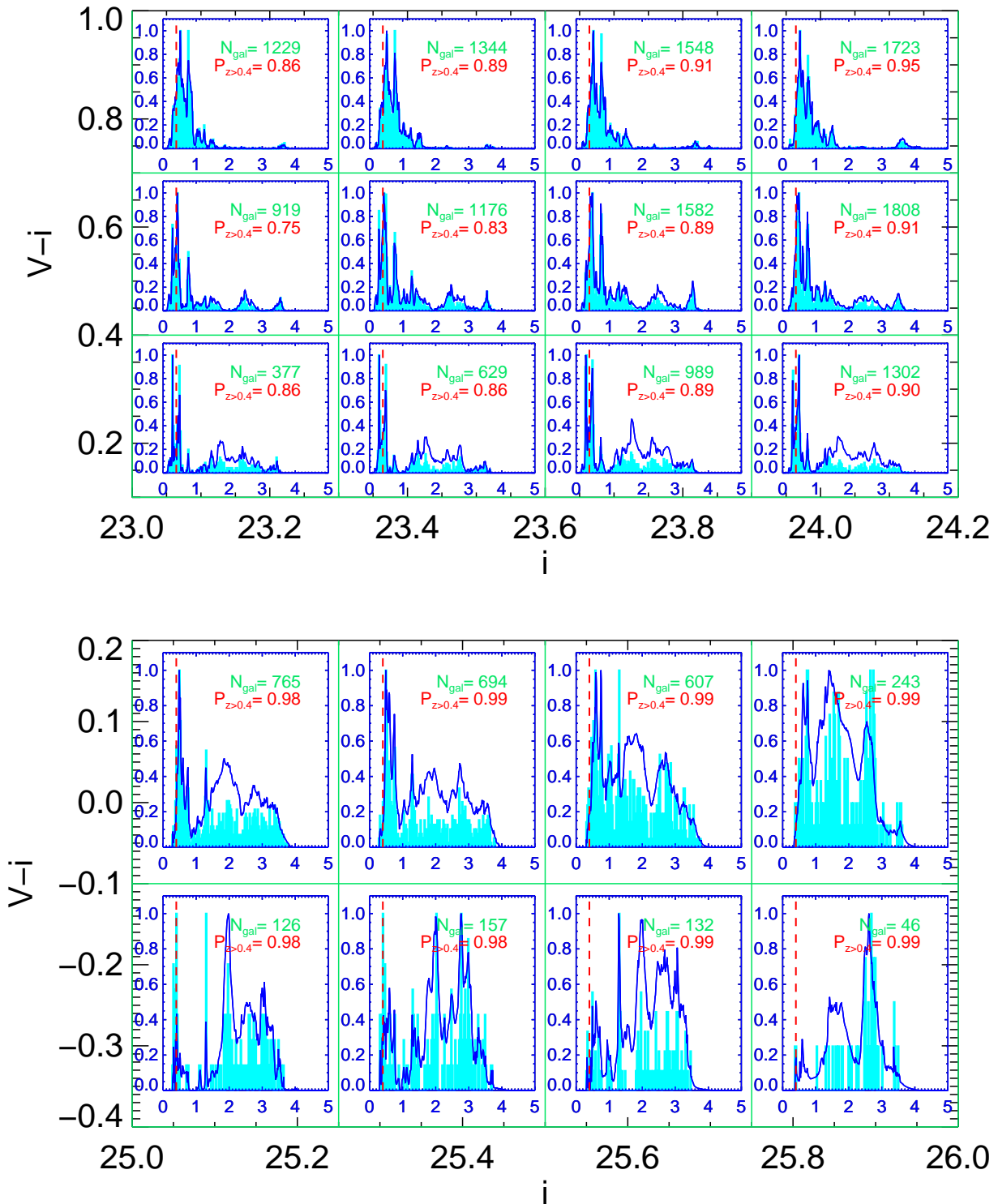


Figure A2. Same as Fig. A1 but for green valley galaxies (top panel) and faint blue galaxies (bottom panel).